Radiation Physics and Chemistry 220 (2024) 111683

Contents lists available at ScienceDirect

Radiation Physics and Chemistry

journal homepage: www.elsevier.com/locate/radphyschem

Enhancing radiation shielding transmission factors and mechanical Robustness of borosilicate glasses through Bi_2O_3 modification: A comprehensive study

Nouf Almousa [a], Shams A.M. Issa [b], H.O. Tekin [d,e], Y.S. Rammah [f], A.M.A. Mostafa [g], Duygu Sen Baykal [h], K. Alshammari [i], Hesham M.H. Zakaly [c,j,*]

[a] Department of Physics, College of Science, Princess Nourah Bint Abdulrahman University, P.O. Box 84428, Riyadh, 11671, Saudi Arabia
[b] Physics Department, Faculty of Science, University of Tabuk, Tabuk, 47512, Saudi Arabia
[c] Physics Department, Faculty of Science, Al-Azhar University, Assiut, 71524, Egypt
[d] Department of Medical Diagnostic Imaging, College of Health Sciences, University of Sharjah, 27272, Sharjah, United Arab Emirates
[e] Istinye University, Computer Engineering Department, Istanbul, 34396, Turkey
[f] Department of Physics, Shebin El-Koom, 32511, Menoufia, Egypt
[g] Physics Department, College of Science, Jouf University, P.O. Box: 2014, Sakaka, Saudi Arabia
[h] Istanbul Kent University, Vocational School of Health Sciences, Medical Imaging Techniques, Istanbul, 34433, Turkey
[i] Department of Physics, Northern Border University, City- Rafha, Saudi Arabia
[j] Institute of Physics and Technology, Ural Federal University, 620002, Ekaterinburg, Russia

ARTICLE INFO

Handling editor: Piotr Ulanski

Keywords:
BaO-ZnO-SiO_2-Sb_2O_3–B_2O_3/Bi_2O_3 glass system
Elastic moduli
Radiation shielding
Monte Carlo code

ABSTRACT

The mechanical behavior and gamma radiation attenuation features of borosilicate glasses with chemical compositions $16ZnO–8BaO-5.5SiO_2-0.5Sb_2O_3-(70-x)B_2O_3/xBi_2O_3$ are extensively investigated. Makishima-Mackenzie principle, Monte Carlo code, and Phy-X/PSD software are utilized in terms of determining these properties. Our results showed that the total packing density (V_t) decreased from 0.634851 to 0.571458, while the total dissociation energy increased from 26.612 (kJ/cm^3) to 29.652 (kJ/cm^3) for S1-glass (with 10 mol% of Bi_2O_3) and S5-glass (with 30 mol% Bi_2O_3). All elastic moduli are enhanced by increasing the Bi_2O_3 additive in the investigated glasses. Poisson's ratio was decreased from 0.281226 for S1-glass to 0.256957 for S5-glass. In terms of gamma-ray shielding parameters; linear (μ) and mass attenuation (μ_m) coefficients for the rich glass sample with B_2O_3 (S5) possess the highest values among all investigated (S1–S5) samples. The glass sample S5 is reported with the lowest values of tenth (TVL) and half (HVL) value layers among all studied glasses. In addition, the exposure (EBF) and energy absorption (EABF) bulidup factors were decreased with increasing the amount of Bi_2O_3 reinforcement for mean free path values from 0.5 to 40 mfp. The lowest possible levels of attenuation (minimum transmission) were measured at a thickness of 3 cm for all of the glass samples.

1. Introduction

Health, industry, and agriculture all benefit from the use of ionizing radiation. Radiation leakage is one of the most serious threats to global health and safety in this regard (Møller and Mousseau, 2013). There are several shielding applications where traditional concrete and lead (Pb) have been employed for many years (AbuAlRoos et al., 2019; Zakaly et al., 2020). Lead, on the other hand, has been related to several long-term problems (Eid and Neurotoxicology, 2016; Hsiao et al., 2011; Ogawa et al., 2008a). Lead in shielding applications, for example, may produce "lead dust," which can be transported home and exposed to children (Ogawa et al., 2008b).

Ongoing research continues to focus on developing radiation shields that are both safe and environmentally friendly while also being affordable. Various materials such, as polymers, metal alloys and glasses show potential, to provide solutions for this purpose (Ahmed et al., 2020; Han and Demir, 2009; Ilik et al., 2022; Kaur et al., 2019; Manjunatha et al., 2019; Mann et al., 2015a; Sayyed, 2016). When considering materials, for radiation shields in the future one material that stands out is borate oxide (Bi_2O_3). It is attractive due to its affordability,

* Corresponding author. Physics Department, Faculty of Science, Al-Azhar University, Assiut, 71524, Egypt.
E-mail addresses: h.m.zakaly@gmail.com, h.m.zakaly@azhar.edu.eg (H.M.H. Zakaly).

https://doi.org/10.1016/j.radphyschem.2024.111683
Received 25 September 2022; Received in revised form 10 February 2024; Accepted 9 March 2024
Available online 19 March 2024

Table 1
Samples code, elemental weight fraction, density, and molar volume of (70-x)B_2O_3–16ZnO–8BaO-5.5SiO_2-0.5Sb_2O_3- xBi_2O_3: (x = 10, 15, 20, 25, 30 mol% glasses.

Samples Code	Elemental weight fraction (Wt.%)							Density, ρ (g/cm^3)(Liu et al., 2022)	Molar volume, V_m (cm^3/mol)(Liu et al., 2022)
	B	O	Si	Zn	Ba	Sb	Bi		
S1	0.109547	0.333045	0.013045	0.08834	0.092779	0.010282	0.352962	4.111	28.8052
S2	0.086022	0.2853	0.011175	0.075676	0.079478	0.008808	0.453542	4.6973	29.4286
S3	0.068397	0.249527	0.009773	0.066187	0.069513	0.007704	0.528899	5.0905	31.048
S4	0.054698	0.221726	0.008684	0.058813	0.061768	0.006846	0.587465	5.5821	31.8641
S5	0.043747	0.199499	0.007814	0.052917	0.055576	0.006159	0.634288	5.8391	33.8555

ease of production transparency, and heat resistance several (Al-Buriahi and Rammah, 2019; Alsaif et al., 2023; Boodaghi Malidarre et al., 2023a; Gomaa et al., 2023; Kurudirek, 2017; Sayyed et al., 2018). The hygroscopic nature of borate makes it difficult to produce a stable glass. The issue may be resolved by using the relevant modifiers at the correct concentrations. The high effective atomic number of some heavy modifiers, such as bismuth, barium, cadmium, molybdenum, and tungsten, makes them excellent absorbers of ionizing radiation (Al-Hadeethi et al., 2020; ALMisned et al., 2021a; Issa et al., 2022; Mostafa et al., 2024; Tekin et al., 2022b; Zakaly et al., 2021b). Other light elements like sodium and calcium have also been utilized to increase the stability of a product. Borosilicate glasses are those that include both SiO_2 and B_2O_3. Due to its high constancy versus fracture strength and mechanical stress at room temperature, silicate glass has gotten more attention, with high constancy being a critical issue in shielding applications (Deliormanli et al., 2021; Salem et al., 2023; Tekin et al., 2022e; Tekin et al., 2022a). The combination of borate and silicate (borosilicate glass) is more thermal shock resistant than silicate glass alone (Bois et al., 1995). In comparison to other glasses, borosilicate glass has good mechanical qualities (Bois et al., 1995; Chanthima and Kaewkhao, 2013; Singh et al., 2014). Adding heavy metal oxides like bismuth oxide (Bi_2O_3) to borosilicate glasses reduces phonon energy, enhancing chemical durability and radiation shielding effectiveness. Bi_2O_3 boasts several advantages: low toxicity, low melting point, stable chemistry, and a PbO-like structure that improves adhesion and reduces softening (Khanna et al., 1996; Singh et al., 2003, 2004). Antimony oxide (Sb_2O_3) is another promising modifier with desirable properties like high refractive index, polarizability, and phonon emission. Studies combining Sb_2O_3 with borate glass show potential in both optical and radiation shielding applications (Kilic et al., 2021; Som and Karmakar, 2011). Antimony (Sb) acts as a modifier to improve the stability and density of types of glasses. Barium oxide (BaO) is known for its properties. Including BaO does not enhance the density of the material. Also improves its mass attenuation coefficient, making it highly important, for applications involving radiation shieldin (He et al., 2019; Shaaban et al., 2009). ZnO-containing optical materials have been getting a lot of interest from the scientific community all over the world because of their unique optical features as well as their non-toxicity, non-hygroscopic nature, and reduced cost. Zinc oxide (ZnO) is often combined with borate to increase the glass system's resilience to chemical degradation, thermal instability, and crystallization (Alfryyan et al., 2023; Zaid et al., 2012). This study aimed to investigate the mechanical behavior and radiation attenuation properties of several types of borosilicate glasses. The findings may help with the investigation of the change in mechanical and gamma-ray attenuation behaviors of glasses based on various kinds of modifications.

2. Research approach and methodology

This study focuses on evaluating the effects of incorporating bismuth oxide into a borosilicate glass matrix, specifically targeting (i) the material's mechanical attributes and (ii) its efficiency in shielding against gamma radiation. The choice of borosilicate glass as the foundational material stems from its noted enhancement in mechanical strength upon the addition of heavy metal oxides. The composition, including density and molar volume, of the glass samples comprising BaO–ZnO–SiO_2–Sb_2O_3–B_2O_3/Bi_2O_3, is documented in Table 1. The anticipated outcome of introducing bismuth oxide into these glasses is a notable increase in their density, which in turn is expected to bolster their capabilities in blocking gamma radiation.

Besides employing the Makishima-Mackenzie (MM) principle for assessing mechanical attributes (Elkhoshkhany et al., 2020; Inaba et al., 1999; Makishima and Mackenzie, 1973; Zakaly et al., 2023a, 2023b), this study also engaged Monte Carlo simulations (computer code Collection, R, 2002) and various theoretical analytical methods (Şakar et al., 2020)to evaluate the shielding properties and calculate the gamma-ray transmission factor (TF) values. The visual representation of the Monte Carlo N-Particle eXtended (MCNPX) simulation setup is illustrated in Fig. 1, showcasing both two-dimensional and

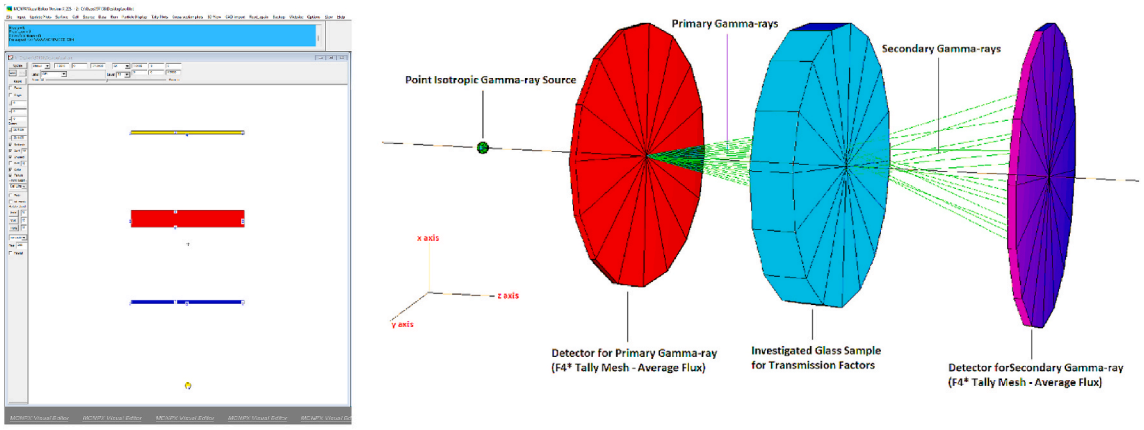

(a) **(b)**

Fig. 1. (a) 2-D view of designed MCNPX simulation setup **(b)** 3-D illustration of designed MCNPX setup (2-D and 3-D views are obtained from MCNPX Visual Editor VisedX22S).

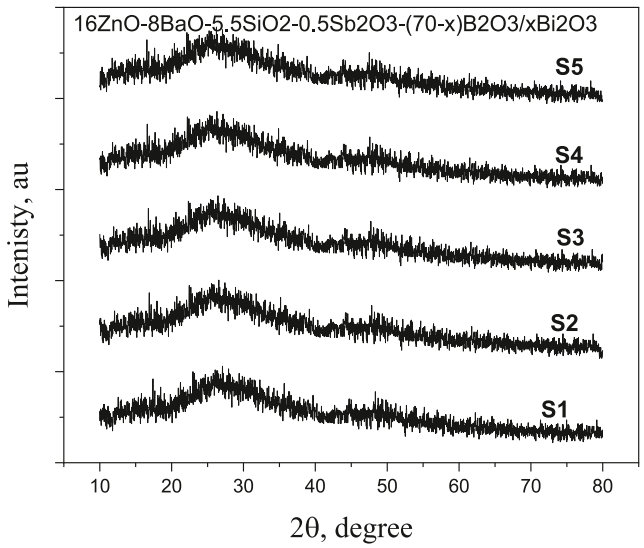

Fig. 2. XRD pattern of the investigated glasses.

three-dimensional perspectives. Specifically, Fig. 1a provides a basic view of the simulation environment, while the enhanced version created using the MCNPX visual editor is presented, offering a more detailed and rendered visualization of the simulation layout. Fig. 1b further illustrates the three-dimensional configuration of the experimental setup, highlighting the placement of the glass sample used as a radiation attenuator, alongside the zones allocated for detecting primary photons emitted from the radiation source and secondary photons that have been attenuated by passing through the glass sample.

In the current investigation, X-ray diffraction (XRD) was employed to analyze the structural properties of the five bismuth borosilicate glass samples, with a fundamental composition of 16ZnO–8BaO-5.5SiO_2-0.5Sb_2O_3 and variable B_2O_3/Bi_2O_3 ratios. The Bi_2O_3 content in these glasses ranged from 10 to 30 mol%, increasing in increments of 5 mol%, as inspired by methodologies outlined in previous research (Liu et al., 2022). Each sample was uniquely identified, with their respective densities and molar volumes as follows: Sample S1 contained 10 mol% Bi_2O_3, resulting in a density of 4.111 g/cm^3 and a molar volume of 28.8052 cm^3/mol. Sample S2, with 15 mol% Bi_2O_3, had a density of 4.6973 g/cm^3 and a molar volume of 29.4286 cm^3/mol. For sample S3, the Bi_2O_3 content was 20 mol%, yielding a density of 5.0905 g/cm^3 and a molar volume of 31.048 cm^3/mol. Sample S4 comprised 25 mol% Bi_2O_3, which contributed to its density of 5.5821 g/cm^3 and molar volume of 31.8641 cm^3/mol. Finally, sample S5, with the highest Bi_2O_3 concentration of 30 mol%, exhibited a density of 5.8391 g/cm^3 and a molar volume of 33.8555 cm^3/mol. The specific details regarding the elemental weight fraction and additional characteristics of these samples were meticulously catalogued in Table 1. Fig. 2 illustrates the XRD patterns of these investigated glasses, exhibiting the characteristic broad humps and the absence of sharp peaks, which are indicative of their amorphous nature. The broad humps increase in intensity with higher Bi_2O_3 content, suggesting changes in the glass structure as more Bi2O3 is incorporated. This absence of crystalline peaks confirms the amorphous structure of all glass samples, with varying Bi_2O_3 concentrations having no significant impact on the amorphous state of these materials.

2.1. Mechanical properties of bismuth borosilicate glasses (S1–S5)

In this study, the elastic moduli and Poisson's ratio of the investigated bismuth borosilicate glasses (S1–S5) were examined via Makishima-Mackenzie (MM) principle (Inaba et al., 1999; Issa et al., 2023; Makishima and Mackenzie, 1973; Zakaly et al., 2023a). The main issue in the MM principle is calculating the total ionic packing density

Table 2
Packing density factor (V_i), and dissociation/bond energy per unit volume (G_i) of the oxides Bi_2O_3, B_2O_3, BaO, ZnO, SiO_2, and Sb_2O_3.

Oxide	V_i (cm^3/mol) [39]	G_i (kJ/cm^3) [39]
Bi_2O_3	26.1	31.6
B_2O_3	20.8	16.4
BaO	13.1	40.6
ZnO	7.9	41.5
SiO_2	14	64.5
Sb_2O_3	23	35.3

(V_t) and the total dissociation energy per unit volume (G_t) for the glass system oxides using the following relations (Inaba et al., 1999; Makishima and Mackenzie, 1973; Zakaly et al., 2023b, 2023c):

$$V_t = \left(\frac{1}{V_m}\right)\sum_i (V_i x_i) \tag{1}$$

$$G_t = \sum_i (G_i x_i)\ \left(\mathrm{kJ}\,/\,cm^3\right) \tag{2}$$

Where, (V_i) is the packing density factor and (G_i) is the dissociation energy per unit volume of the contributed glass systems oxides.

Then, elastic moduli (Young's (E_{MM}), bulk (K_{MM}), shear (S_{MM}), and longitudinal (L_{MM})) can be calculated in GPa unit via the next relations (3–6), respectively (Inaba et al., 1999; Makishima and Mackenzie, 1973; Zakaly et al., 2023b, 2023c):

$$E_{MM} = 2V_t G_t \tag{3}$$

$$K_{MM} = 1.2 V_t E_{MM} \tag{4}$$

$$S_{MM} = \frac{(3E_{MM}K_{MM})}{(9K_{MM} - E_{MM})} \tag{5}$$

$$L_{MM} = K_{MM} + \frac{4}{3}S_{MM} \tag{6}$$

Also, Poisson's ratio (σ_{MM}) can be calculated via:

$$\sigma_{MM} = \left(\frac{E_{MM}}{2G_{MM}}\right) - 1 \tag{7}$$

3. Results and discussion

3.1. Assessment of mechanical properties (elastic moduli and Poisson's ratio)

We estimated the fundamental mechanical parameters of the examined glasses using the fundamental calculation parameters reported in Table 2. On the other hand, Table 3 displays the calculated values of (V_t) and (G_t). Using data from Table 3, one can see that the (V_t) and (G_t) values for S1–S5 glasses fall from 0.634851 for S1-glass (10 mol % of Bi_2O_3) to 0.571458 for S5-glass (30 mol% of Bi_2O_3) Fig. 3. This drop might be interpreted as a result of the reduced ionic radius of Bi_2O_3 compared to Bi_2O_3. Consequently, as shown in Fig. 3, the (Gt) of the studied glasses rose with increasing the Bi_2O_3 concentration, from a low of 26.612 (*kJ*/cm^3) for S1-glass (with 10 mol% of Bi_2O_3) to a high of 29.652 (*kJ*/cm3) for S5-glass (with 30 mol% of Bi_2O_3). The trend of the (G_t) is due to the replacement of B_2O_3 with low dissociation energy (16.4 kJ/cm^3) by Bi_2O_3 with high dissociation energy (31.6 kJ/cm^3). By applying the obtained values of the (V_t) and (G_t) in relation (3), the values of Young's elastic modulus (E_{MM}) can be obtained, its values were changed from 33.78929 GPa to 34.60428 GPa. Then substituting by (E_{MM}) in relation (4), the bulk elastic modulus ((K_{MM}) of the investigated S1–S5 glasses, its values varied from 23.23989 GPa to 24.86757 GPa. Correspondingly, shear (S_{MM}) and longitudinal (L_{MM}) elastic moduli were computed via relations (5) and (6), respectively. Values of the

Table 3
Total ionic packing density (V_t), total dissociation energy (G_t), Young's modulus ($E_{M\text{-}M}$), bulk modulus ($K_{M\text{-}M}$), shear modulus ($S_{M\text{-}M}$), and Poisson's ratio ($\sigma_{M\text{-}M}$) based on Makishima-Mackenzie model of the studied glasses. The x_i is mole fraction of the component i of an oxide glass and V_m is the molar volume of the glass samples.

Parameters and elastic moduli	S1	S2	S3	S4	S5
$V_t = \left(\frac{1}{V_m}\right)\sum_i (V_i x_i)$	0.634851	0.630407	0.606062	0.598856	0.571458
$G_t = \sum_i (G_i x_i)$ (kJ/cm^3)	26.612	27.372	28.132	28.892	29.652
$E_{MM} = 2V_t G_t$ (GPa)	33.78929	34.51101	34.09945	34.60428	33.88975
$K_{MM} = 1.2V_t E_{MM}$ (GPa)	25.74138	26.10718	24.79964	24.86757	23.23989
$S_{MM} = \frac{(3E_{MM}K_{MM})}{(9K_{MM} - E_{MM})}$ (Gpa)	13.18631	13.48419	13.41617	13.6444	13.48087
$L_{MM} = K_{MM} + \frac{4}{3}S_{MM}$ (Gpa)	43.27918	44.04116	42.64315	43.01462	41.16945
$\sigma_{MM} = \left(\frac{E_{MM}}{2G_{MM}}\right) - 1$ (GPa)	0.281226	0.279684	0.270834	0.268076	0.256957

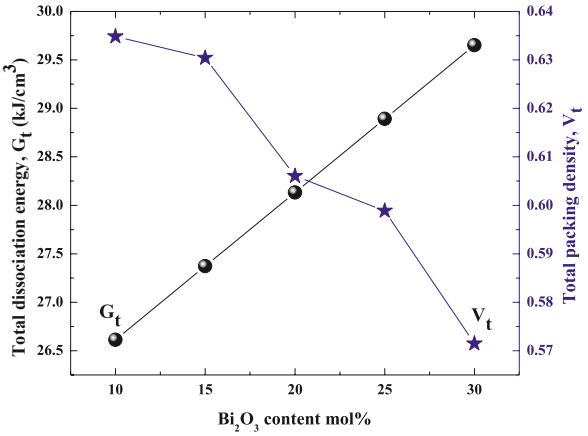

Fig. 3. Variation of G_t and V_t as a function of Bi_2O_3 content mol% of the investigated glasses.

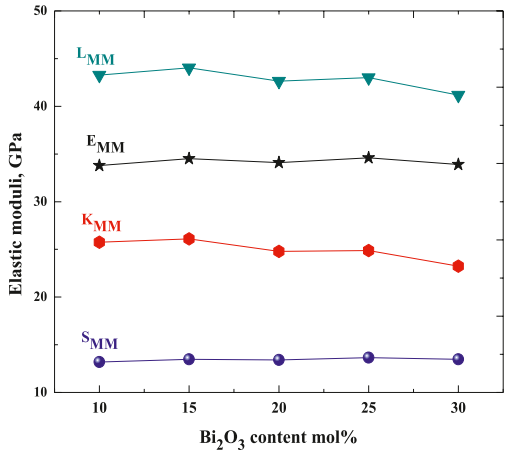

Fig. 4. Variation of elastic moduli as a function of Bi_2O_3 content mol% of the investigated glasses.

shear (S_{MM}) were changed from 13.18631 GPa to 13.6444 GPa, while values of the (L_{MM}) were varied from 41.16945 GPa to 44.04116 GPa as shown in Fig. 4. Poisson's ratio of the studied S1–S5 glasses is computed via relation (7), the values of (σ_{MM}) are decreased from 0.281226 for S1-glass to 0.256957 for S5-glass as shown in Fig. 5. The observed variation in the mechanical features of the studied glasses may be attributed to the increase in vacancies, defects, and creation of a large number of non-bridging oxygen (NBO) with increasing Bi_2O_3 content in glasses (Boodaghi Malidarre et al., 2023b; Issa et al., 2020; Rammah et al., 2021; Zakaly et al., 2023a).

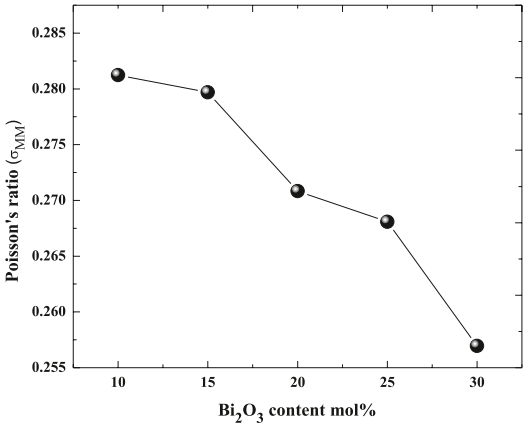

Fig. 5. Variation of Poisson's ratio as a function of Bi_2O_3 content mol% of the investigated glasses.

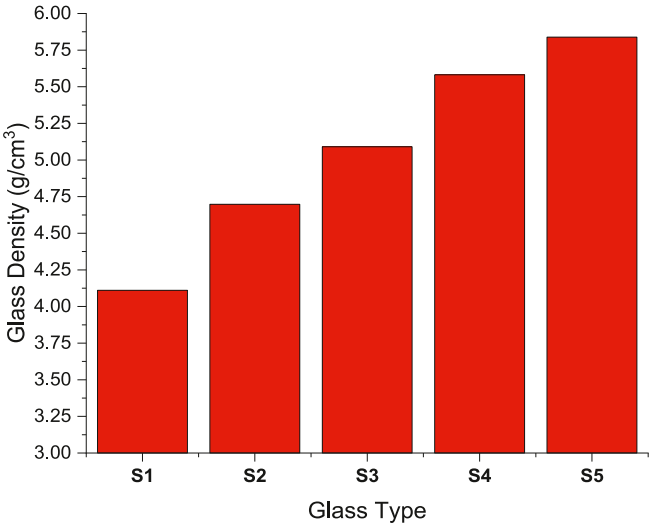

Fig. 6. Describes differences among densities of glass types.

3.2. *Gamma-ray shielding properties*

Five distinct glass samples were tested for shielding characteristics against ionizing gamma rays in the second part of the study of the examined bismuth borosilicate glass group. Fig. 6 depicts the change in the density of the examined glass group. From sample S1 to sample S5, the glass density increased, as seen in the figure. Due to a progressive increase from sample to sample, the Bi additive rate in S5 (0.634288 wt

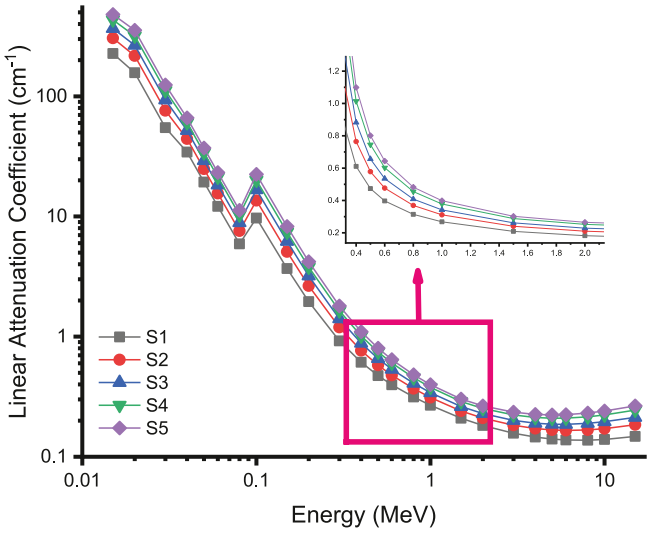

Fig. 7. Variations of linear attenuation coefficient (cm^{-1}) with photon energy (MeV) for all S1–S5 glasses.

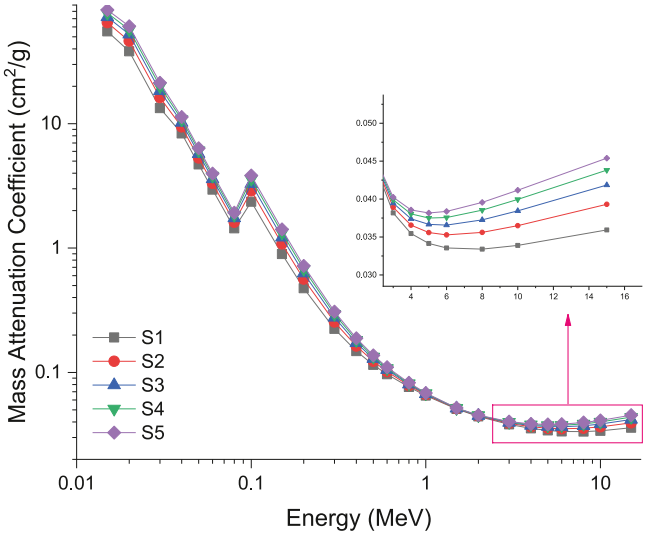

Fig. 8. Variations of mass attenuation coefficients (cm^2/g) with photon energy (MeV) for all S1–S5 glasses.

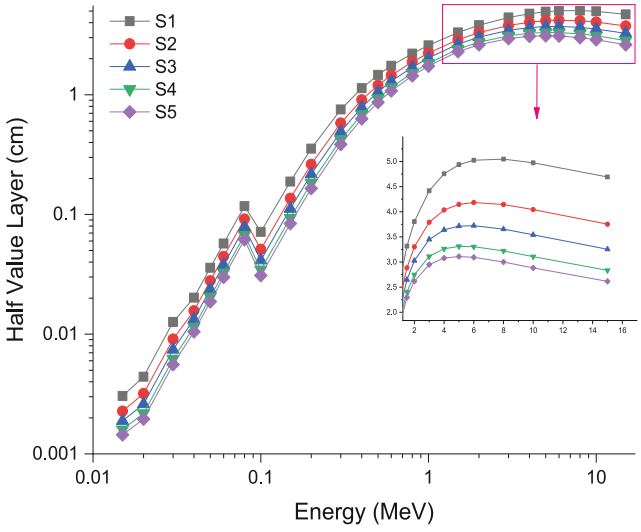

Fig. 9. Variations of half value layer (cm) with photon energy (MeV) for all S1–S5 glasses.

% out of 1) is the highest of any sample studied. The S5 sample's maximum glass density was determined to be 5.8391 g/cm^3 due to the impact of the highest Bi additive (Liu et al., 2022). To further investigate the effect of material density on a key parameter, the phrase linear attenuation coefficient (μ) might be employed. Variations in linear attenuation coefficient and representation as a function of increasing energy values are shown in Fig. 7. In the interaction process of energetic photons with matter, different mechanisms may become dominant. This situation changes according to the magnitude of the energy possessed by the photons interacting with the matter. When it comes to low-energy photon interactions, for example, the photoelectric effect is by far the most frequent (H. O. Tekin et al., 2022e; Tekin et al., 2021; Almisned et al., 2021b). According to recent findings, the linear attenuation coefficients in the low-energy region have begun to decline dramatically, as seen in Fig. 7. A k-absorption peak of Bi was also observed and linear attenuation coefficient values continued their downward trend after this drop. For the S5 glass sample, we found the highest linear attenuation coefficients of all those examined. Because of the above-mentioned maximum Bi contribution and the additive's indirect influence on glass density, this situation is reported for linear attenuation coefficients (Khalil et al., 2024; Zakaly et al., 2021a). The mass attenuation coefficient (μ_m) was then calculated as a density-independent shielding parameter. Fig. 8 displays the mass attenuation coefficients for all glasses in the S1–S5 series. Our findings showed that the S5 sample exhibited the highest mass attenuation coefficient among the evaluated glasses. Mass attenuation coefficients for S5 may have been changed by the increased proportion of Bi in the structure, as a result of Bi's higher atomic number (Ali et al., 2023). By altering the thickness of the material, one may adjust the amount of gamma radiation that passes through. The relative attenuation performances of different attenuator samples relative to the same gamma-ray energy level is another standard by which to evaluate attenuator samples. In order to determine a

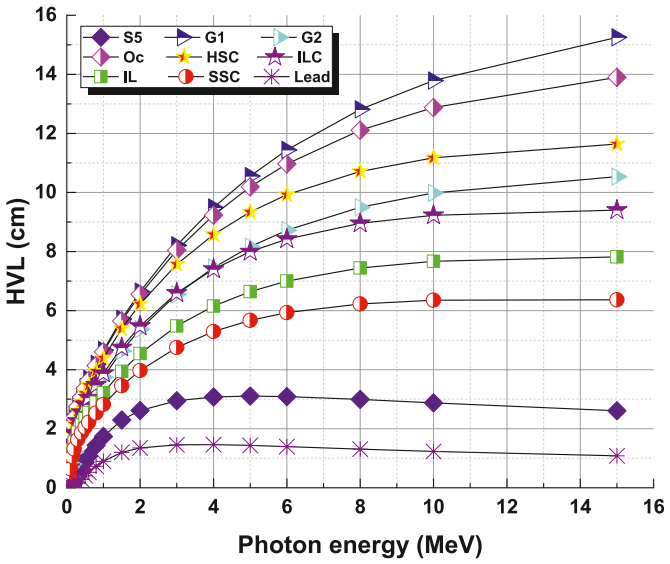

Fig. 10. Comparison of half-value layer (HVL) for S5 glass with Bi_2O_3 against traditional and novel shielding materials.

shielding material's half-value layer (HVL) value, directly measuring the thickness of the material in centimetres at which the gamma ray's energy is reduced by half. The HVL values of the glass samples investigated in this study were determined at energies between 0.015 and 15 MeV for samples S1, S2, S3, S4, and S5 are shown against incoming gamma-ray energy in Fig. 9. With increasing half-value layer thickness, the glass samples clearly exhibited different behaviors. For instance, half-value thicknesses are very small in the low-energy zone and get gradually bigger when energy is applied. All of the tested glass samples had extremely low HVL needs for the low energy zone because of their density and weight. These HVL values, however, soared to higher values (cm) in the high-energy zone, as seen in the graph Among all energy levels, the S5 sample has the lowest HVL values, as can be seen in Fig. 9. Particularly concerning the effect of Bi_2O_3 augmentation on borosilicate glass properties and their comparison to similar glass compositions and traditional shielding materials Fig. 10, our study undertakes an extensive evaluation. We have incorporated detailed comparative figures to elucidate the half-value layer (HVL) values of our most effective glass sample (S5), juxtaposed against an array of other shielding materials. These include conventional options such as lead and various forms of concrete—ordinary, (HSC), and (ILC)—as well as innovative materials like iron limonite (IL), steel slag concrete (SSC), and two distinct glass formulations, G1 and G2 (Bashter, 1997; Issa et al., 2018). This comparative analysis aims to underscore the gamma-ray attenuation prowess of our S5 sample, delineating its superiority or competitive stance vis-à-vis both traditional and novel shielding contenders. By integrating this comparison alongside an analytical discourse, we aim to illuminate the transformative influence of Bi_2O_3 integration on the radiation shielding efficacy of borosilicate glasses. This approach addresses the previously highlighted gap and enriches the manuscript by casting our results against a broader scholarly backdrop. The juxtaposition delineates the promising potential of Bi_2O_3-doped borosilicate glasses as an innovative substitute for age-old radiation shielding materials, shedding light on their practical benefits and positioning within the spectrum of radiation protection solutions.

On the other hand, it is possible to employ a tenth value layer (TVL) to construct a new component that is similar to the half-value layer and provides equal operational information. Like HVL, this metric specifies how thick a layer of material must be to reduce radiation intensity by 10% (Rammah et al., 2020; H. O. Tekin et al., 2022e). The tested TVL values for heavy metal oxide glasses are shown to change as a function of energy in Fig. 11. The tenth value layer values are quantitatively greater than the half-value layer values for the identical energy values. This occurs often, and additional shielding material is required to lower the radiation by one-tenth. While the quantitative values for qualities like these are different for comparable energy values, it turns out that the S5 sample has the lowest values in one-tenth value thickness. Once radiation has made first contact with the shielding material and penetrated into the interior areas, individual photons will interact with atoms inside the substance. Incoming radiation undergoes these interactions, which result in its energy being completely absorbed. Mean free path (mfp) is a parameter used to calculate the minimum distance between two consecutive photon interactions in a material. For a given energy value, calculating the mean free path gives valuable insight into how variations in addition to incorporation and chemical composition affect the following contact distance between the photon and matter, making it an

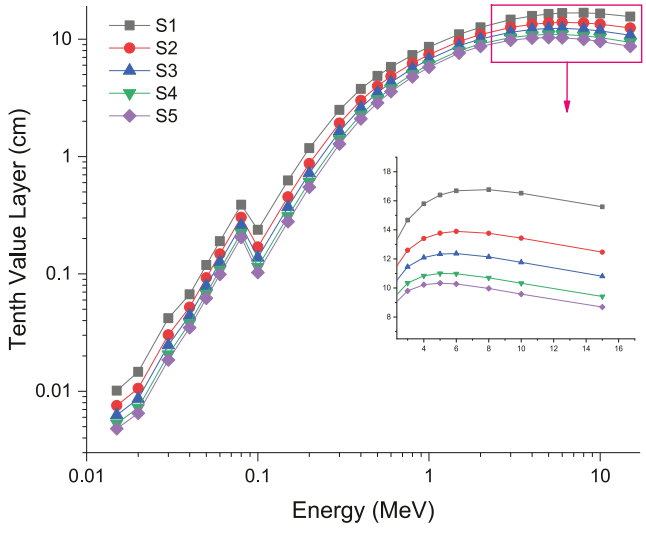

Fig. 11. Variations of tenth value layer (cm) with photon energy (MeV) for all S1–S5 glasses.

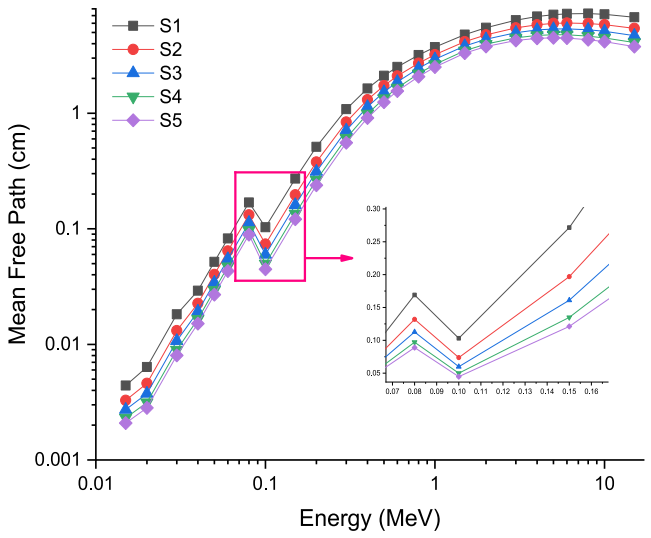

Fig. 12. Variations of mean free path (cm) with photon energy (MeV) for all S1–S5 glasses.

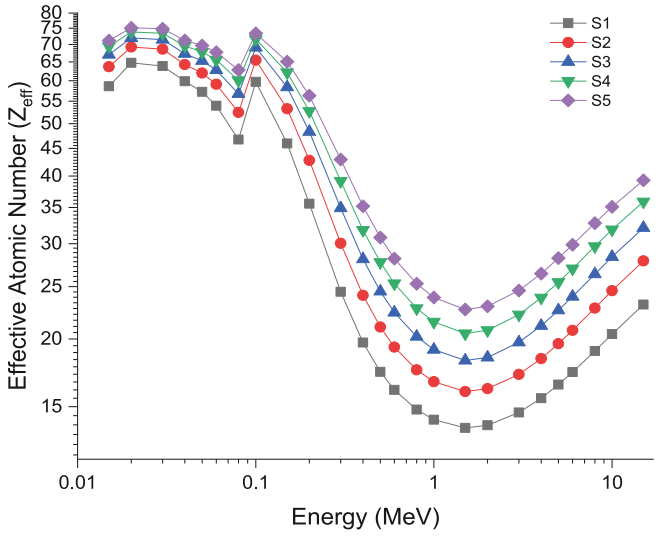

Fig. 13. Variations of effective atomic number (Z_{eff}) with photon energy (MeV) for all S1–S5 glasses.

invaluable tool for comparative studies. Fig. 12 depicts the variation in the mean free path for different photon energies for glasses in the S1–S5 range (MeV). The measured mean free path values for the glass samples vary with the photon energy (see Fig. 12). This seems to indicate a correlation between the average range of a gamma ray and its ability to penetrate matter. Gamma radiation has increasing mean free path values with increasing energy, however, the S5 sample had the lowest mean free path values for any given gamma radiation energy. To put it another way, the S5 sample is more efficient at absorbing gamma rays of a given energy when they are nearby. In general, an effective atomic number (Z_{eff}) is used to calculate the mean atomic number of a compound or mixture of substances. Moreover, Z_{eff} is helpful not just for comprehending why electrons farther out from the nucleus are so much weaker coupled than those closer to the nucleus, but also for determining when to utilize simpler techniques for computing other characteristics and interactions (ALMisned et al., 2021a; Mahmoud et al., 2021; Mann et al., 2015b; Tekin et al., 2022d; Zakaly et al., 2022). In this study, Z_{eff} values of S1, S2, S3, S4, and S5 samples were determined in 0.015–15 MeV energy range. Z_{eff} shifts as a function of photon energy

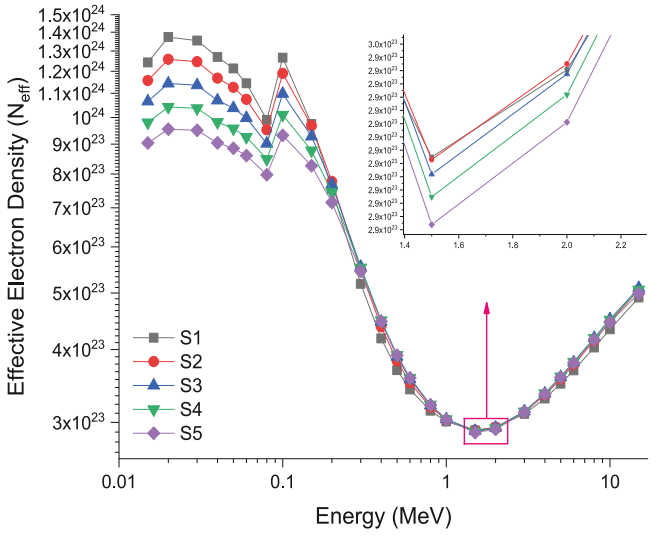

Fig. 14. Variations of effective electron density (electrons/g) with photon energy (MeV) for all S1–S5 glasses.

are seen in Fig. 13 for all S1–S5 glasses. Z_{eff} values were found to be greatest in the low-energy zone, where the photoelectric effect between the incoming photon and matter was most prevalent. Z_{eff} increased significantly in the lowest energy range as a result of increasing Bi contribution in the glass structure. This can be explained by the high atomic number (i.e., 81) of Bi element. After that, the intensity of Compton scattering within the mid-energy band dramatically reduced the Z_{eff} values. The results obtained indicated that the S5 sample had the highest Zeff values because it included the highest mass attenuation coefficients and the highest Bi incorporation in the glass matrix. The effective electron density (N_{eff}) is strongly linked to the effective atomic number. For all glasses, the effective electron density (electrons/g) is shown in Fig. 14. A similar trend in the energy-dependent variation of the N_{eff} values may be attributed to the fact that the values of the effective atomic number and electron density, known as Z_{eff} and N_{eff}, are exactly proportional. Our results revealed that the S5 sample, which has the highest effective atomic number among the examined glass samples, also has the highest effective electron density. A common term for the proportion of one's overall exposure that comes from unscattered radiation is build-up factor (E,x). Accordingly, the buildup factor has to be considered while designing shielding for radioactive sources like nuclear reactors. Medical radiation barriers need to compensate for the build-up factor so that they can better understand how the shield material reacts to incoming gamma rays. When the scattering cross section is small relative to the absorption cross section, the build-up factors become large, sometimes even surpassing zero. Fig. 15 and Fig. 16 depict the gamma-ray energy (MeV) over the mean free path (MFP) dependence of the energy absorption build-up factor (EABF). Absorption of incoming gamma rays is dominated by photoelectric interaction, as shown by the very small EBF and EABF values in the low gamma ray energy area. Compton Scattering, however, causes a significant increase in both the EBF and EABF values by around 0.1 MeV. Increasing the amount of Bi_2O_3 reinforcement decreased the EBF and EABF values for all mean free pathways, as shown by our findings. As the amount of Bi in the glass samples grows from S1 to S4, the collision rate of incoming gamma rays increases considerably.

The gamma-ray transmission factor (TF), a crucial parameter for assessing the effectiveness of shielding materials, was evaluated across a range of energies corresponding to common radioisotopes. These energies included 0.0086 MeV, 0.0093 MeV, and 0.1840 MeV for Gallium-67 (^{67}Ga); 0.0144 MeV, 0.1221 MeV, and 0.1365 MeV for Cobalt-57 (^{57}Co); 0.5110 MeV and 0.8108 MeV for Cobalt-58 (^{58}Co); 1.1732 MeV and 1.3325 MeV for Cobalt-60 (^{60}Co); a series of energies 0.0532

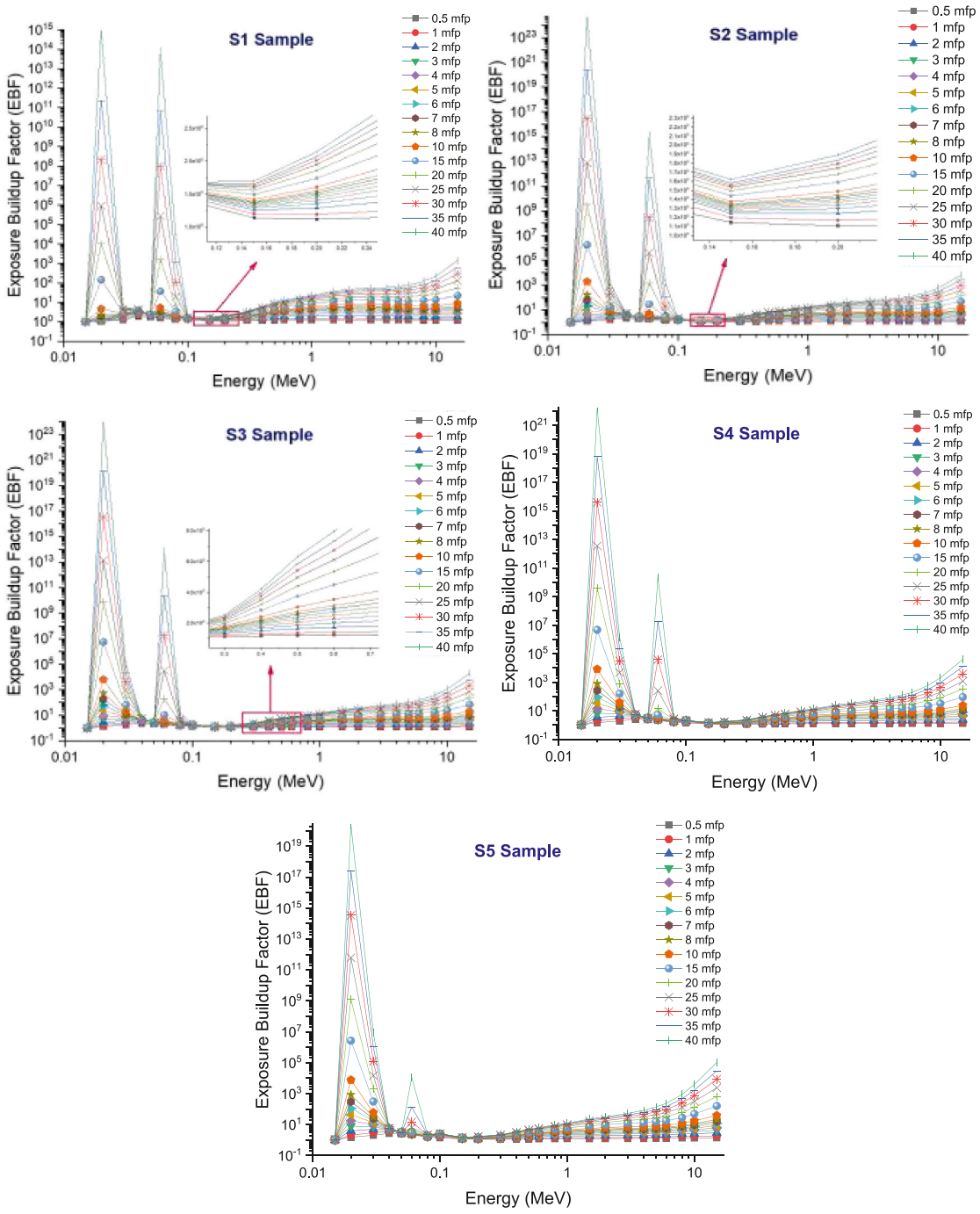

Fig. 15. Variation of exposure buildup factors (EBF) of investigated glasses at different mean free path values.

MeV, 0.0796 MeV, 0.0810 MeV, 0.2764 MeV, 0.3029 MeV, 0.3560 MeV, and 0.3838 MeV for Barium-133 (^{133}Ba); 0.0710 MeV, 0.1350 MeV, and 0.1670 MeV for Thallium-201 (^{201}Tl); 0.0230 MeV, 0.2450 MeV, and 0.1710 MeV for Indium-111 (^{111}In); and for Iodine-131 (^{131}I), the energies were 0.2843 MeV, 0.3645 MeV, 0.6370 MeV, and 0.7229 MeV. Additionally, Technetium-99 m (^{99m}Tc) was tested at 0.1405 MeV, Chromium-51 (^{51}Cr) at 0.3201 MeV, and Cesium-137 (^{137}Cs) at 0.6617 MeV. These specific energy levels were chosen to comprehensively understand the shielding material's performance across a broad spectrum of gamma-ray energies encountered in various radiological applications. Fig. 17 shows the radioisotope energy (MeV) for different glass thicknesses based on the TFs of the studied glasses. The radioisotope's energy causes the transmission factor to increase as well, from 0.0086 MeV to 1.3326 MeV. The glass samples' TF values were the lowest across the board at low energy levels. This is because to the thick samples' superior attenuation of low-energy gamma rays. Nevertheless, at about 0.1 MeV, a distinction becomes evident. The reaction to gamma rays with energy greater than 0.1 MeV varies over a range of glass thicknesses. All of the glasses were tested at a thickness of 3 cm to determine their minimum attenuation (also called minimum transmission). Shielding materials' attenuation capacities may be modified by shield thickness; hence, increasing shield thickness improves the attenuation of inbound gamma rays.

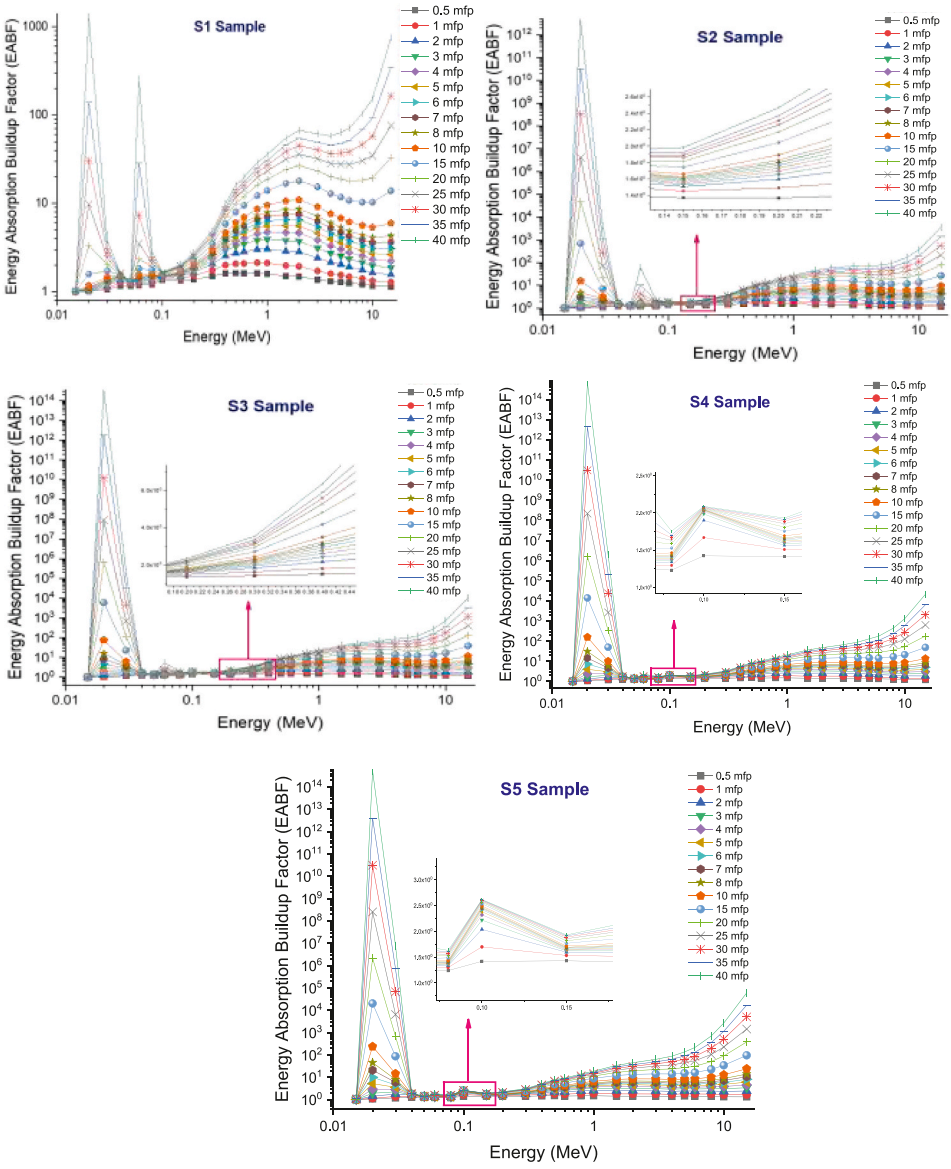

Fig. 16. Variation of energy absorption buildup factors (EABF) of investigated glasses at different mean free path values.

4. Conclusion

This study systematically investigated the impact of increasing Bi_2O_3 content (10–30 mol%) on the mechanical and gamma-ray attenuation properties of borosilicate glasses. Five compositions were synthesized and analyzed using theoretical tools and simulations. To this end, Makishima-Mackenzie principle, Monte Carlo code, and Phy-X/PSD software were applied. Our findings revealed that.

- Packing density Decreased, and dissociation energy Increased, suggesting enhanced structural stability with Bi_2O_3addition.
- Elastic moduli: All (Young's, Shear, Bulk, and Longitudinal) significantly increased with Bi_2O_3 content, indicating improved mechanical strength.
- Gamma-ray shielding: Glass with the highest Bi_2O_3 (S5) showed superior performance and higher linear (μ) and mass attenuation (μm) coefficients. Lower tenth (TVL) and half (HVL) value layers for more efficient absorption (e.g., TVL decreased from 2.92 cm (S1) to 2.25 cm (S5)).
- In addition, the exposure (EBF) and energy absorption (EABF) buildup factors were decreased with increasing the amount of Bi_2O_3 reinforcement for all mean free path values.

Based upon incorporating Bi_2O_3 into glasses significantly enhances their nuclear radiation shielding, with the S5 sample exhibiting superior absorption. While promising, further optimization and research on the material properties' influence are crucial for achieving the suggested glass system's full potential. This work provides a foundation for future investigations into optimizing and enhancing radiation-shielding glasses.

CRediT authorship contribution statement

Nouf Almousa: Validation, Visualization, Writing – review & editing. **Shams A.M. Issa:** Conceptualization, Data curation, Writing – original draft. **H.O. Tekin:** Resources, Validation, Writing – review & editing. **Y.S. Rammah:** Conceptualization, Data curation. **A.M.A. Mostafa:** Resources, Validation, Visualization, Writing – review & editing. **Duygu Sen Baykal:** Formal analysis, Methodology, Resources, Visualization. **K. Alshammari:** Investigation, Methodology, Writing –

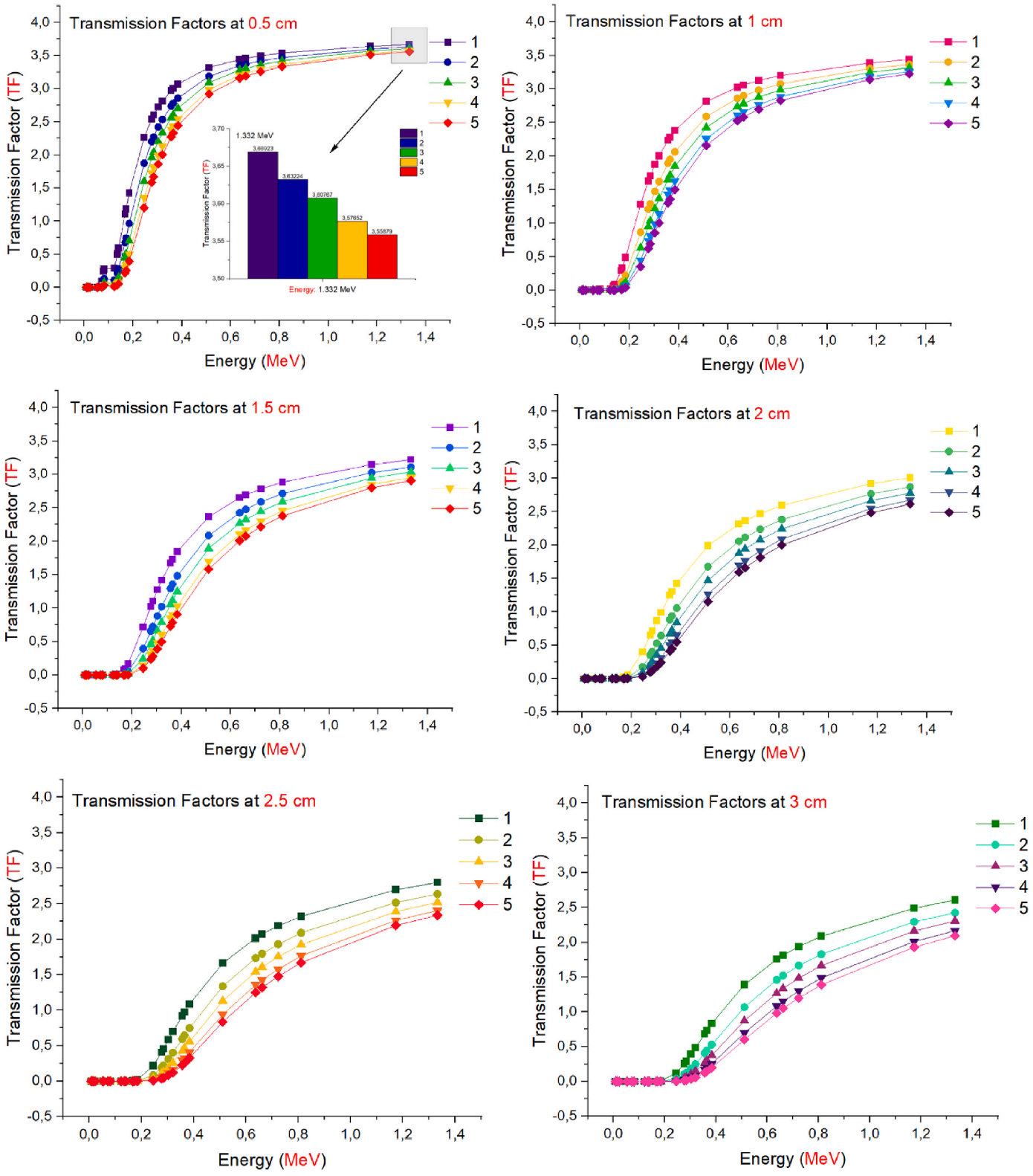

Fig. 17. Comparison of the Transmission Factors (TFs) as a function of used radioisotope energy (MeV) for different glass thicknesses.

review & editing. **Hesham M.H. Zakaly:** Investigation, Methodology, Software, Supervision, Writing – original draft, Writing – review & editing.

Declaration of competing interest

The authors declare that they have no known competing financial interests or personal relationships that could have appeared to influence the work reported in this paper.

Data availability

Data will be made available on request.

Acknowledgements

The authors express their gratitude to Princess Nourah bint Abdulrahman University Researchers Supporting Project (Grant No. PNURSP2024R111), Princess Nourah bint Abdulrahman University, Riyadh, Saudi Arabia. H.M.H Zakaly thanks the Ministry of Science and Higher Education of the Russian Federation (Ural Federal University Program of Development within the Priority-2030 Program) is gratefully acknowledged.

References

AbuAlRoos, N.J., Baharul Amin, N.A., Zainon, R., 2019. Conventional and new lead-free radiation shielding materials for radiation protection in nuclear medicine: a review. Radiat. Phys. Chem. 165, 108439 https://doi.org/10.1016/j.radphyschem.2019.108439.

Ahmed, B., Shah, G.B., Malik, A.H., Aurangzeb, Rizwan, M., 2020. Gamma-ray shielding characteristics of flexible silicone tungsten composites. Appl. Radiat. Isot. 155, 108901 https://doi.org/10.1016/J.APRADISO.2019.108901.

Al-Buriahi, M.S., Rammah, Y.S., 2019. Electronic polarizability, dielectric, and gamma-ray shielding properties of some tellurite-based glasses. Appl. Phys. Mater. Sci. Process 125, 1–9. https://doi.org/10.1007/s00339-019-2976-z.

Al-Hadeethi, Y., Al-Buriahi, M.S., Sayyed, M.I., 2020. Bioactive glasses and the impact of Si3N4 doping on the photon attenuation up to radiotherapy energies. Ceram. Int. 46, 5306–5314. https://doi.org/10.1016/j.ceramint.2019.10.281.

Alfryyan, N., Alrowaili, Z.A., Alomairy, S., Nabil, I.M., Al-Buriahi, M.S., 2023. Radiation attenuation properties of zinc-borosilicate glasses containing Al2O3 and Gd2O3. Silicon. https://doi.org/10.1007/s12633-023-02636-8.

Ali, A.S., Alrowaily, A.W., Issa, S.A.M., Rashad, M., Elsaman, R., Zakaly, H.M.H., 2023. Unveiling the structural, optical, and electromagnetic attenuation characteristics of B2O3–SiO2–CaO–Bi2O3 glasses with varied WO3 content. Radiat. Phys. Chem. 212 https://doi.org/10.1016/J.RADPHYSCHEM.2023.111089.

ALMisned, G., Elshami, W., Issa, S.A.M., Susoy, G., Zakaly, H.M.H., Algethami, M., Rammah, Y.S., Ene, A., Al-Ghamdi, S.A., Ibraheem, A.A., Tekin, H.O., 2021a. Enhancement of gamma-ray shielding properties in Cobalt-doped heavy metal borate glasses: the role of lanthanum oxide reinforcement. Mater 14, 7703. https://doi.org/10.3390/MA14247703, 2021, Vol. 14, Page 7703.

Almisned, G., Tekin, H.O., Bilal, G., Ene, A., Kilic, G., Issa, S.A.M., Algethami, M., Zakaly, H.M.H., 2021b. Trivalent ions and their impacts on effective conductivity at 300 K and Radio-Protective behaviors of bismo-borate glasses: a comparative investigation for Al, Y, Nd, Sm, Eu. Mater 14, 5894. https://doi.org/10.3390/MA14195894, 2021, Vol. 14, Page 5894.

Alsaif, N.A.M., Khattari, Z.Y., Zakaly, H.M.H., Rammah, Y.S., Ene, A., Al-Buriahi, M.S., 2023. Mechanic-elastic properties and radiation attenuation efficiency of TeO2/WO3/K2O composite glass systems for nuclear and medical application. Heliyon 9, e18912. https://doi.org/10.1016/j.heliyon.2023.e18912.

Bashter, I.I., 1997. Calculation of radiation attenuation coefficients for shielding concretes. Ann. Nucl. Energy 24, 1389–1401. https://doi.org/10.1016/S0306-4549(97)00003-0.

Bois, L., Maquet, J., Babonneau, F., Bahloul, D., 1995. Structural characterization of Sol-Gel Derived Oxycarbide glasses. 2. Study of the thermal stability of the Silicon Oxycarbide Phase. Chem. Mater. 7, 975–981. https://doi.org/10.1021/cm00053a025.

Boodaghi Malidarre, R., Akkurt, I., Ekmekci, I., Zakaly, H.M.H., Mohammed, H., 2023a. The role of La2O3 rare earth (RE) material in the enhancement of the radiation shielding, physical, mechanical and acoustic properties of the tellurite glasses. Radiat. Eff. Defect Solid 178, 195–207. https://doi.org/10.1080/10420150.2022.2113075.

Boodaghi Malidarre, R., Akkurt, I., Zakaly, H.M.H., 2023b. Investigation of Ag as chemical modifier in glassy SeTe chalcogenide alloy in terms of radiation shielding, optical, structural, and physical properties. Radiat. Phys. Chem. 204, 110685 https://doi.org/10.1016/J.RADPHYSCHEM.2022.110685.

Chanthima, N., Kaewkhao, J., 2013. Investigation on radiation shielding parameters of bismuth borosilicate glass from 1 keV to 100 GeV. Ann. Nucl. Energy 55, 23–28. https://doi.org/10.1016/J.ANUCENE.2012.12.011.

computer code Collection, R, 2002. MCNPX User's Manual Version 2.4.0 Monte Carlo Particle Transport Code System for Multiple and High Energy Application.

Deliormanli, A.M., Issa, S.A.M., Al-Buriahi, M.S., Rahman, B., Zakaly, H.M.H., Tekin, H. O., 2021. Erbium (III)- and Terbium (III)-containing silicate-based bioactive glass powders: physical, structural and nuclear radiation shielding characteristics. Appl. Phys. Mater. Sci. Process 127. https://doi.org/10.1007/s00339-021-04615-5.

Eid, A., Neurotoxicology, N.Z.-, 2016. Consequences of Lead Exposure, and It's Emerging Role as an Epigenetic Modifier in the Aging Brain. undefined, n.d. Elsevier.

Elkhoshkhany, N., Syala, E., Sayed Yousef, E., 2020. Concentration dependence of the elastic moduli, thermal properties, and non-isothermal kinetic parameters of Yb3+ doped multicomponent tellurite glass system. Results Phys. 16, 102876 https://doi.org/10.1016/J.RINP.2019.102876.

Gomaa, H.M., Saudi, H.A., Yahia, I.S., Zahran, H.Y., Makram, B.M.A., 2023. Effects of Ce2O3 on multi-component borovanadate glass structural, optical, and attenuation characteristics. Radiat. Phys. Chem. 207 https://doi.org/10.1016/j.radphyschem.2023.110847.

Han, I., Demir, L., 2009. Studies on effective atomic numbers, electron densities from mass attenuation coefficients in TixCo1−x and CoxCu1−x alloys. Nucl. Instrum. Methods Phys. Res., Sect. B 267, 3505–3510. https://doi.org/10.1016/J.NIMB.2009.08.022.

He, D., Zhong, H., Gao, C., 2019. Effect of TiO2 doping on crystallization, microstructure and dielectric properties of CBS glass-ceramics. J. Alloys Compd. 799, 50–58. https://doi.org/10.1016/j.jallcom.2019.05.152.

Hsiao, C.L., Wu, K.H., Wan, K.S., 2011. Effects of environmental lead exposure on T-helper cell-specific cytokines in children. J. Immunot. 8, 284–287. https://doi.org/10.3109/1547691X.2011.592162.

Ilik, E., Kilic, G., Issever, U.G., Issa, S.A.M., Zakaly, H.M.H., Tekin, H.O., 2022. Cerium (IV) oxide reinforced Lithium-Borotellurite glasses: a characterization study through physical, optical, structural and radiation shielding properties. Ceram. Int. 48, 1152–1165. https://doi.org/10.1016/J.CERAMINT.2021.09.200.

Inaba, S., Fujino, S., Morinaga, K., 1999. Young's modulus and compositional parameters of oxide glasses. J. Am. Ceram. Soc. 82, 3501–3507. https://doi.org/10.1111/j.1151-2916.1999.tb02272.x.

Issa, S.A.M., Almisned, G., Tekin, H.O., Zakaly, H.M.H., Ene, A., Ibraheemh, A.A., Rammah, Y.S., 2022. Comprehensive evaluation on gamma radiation resistance of chromium (III) ions incorporated bismuth fluoro-lead-borate glasses. Optik 268. https://doi.org/10.1016/J.IJLEO.2022.169809.

Issa, S.A.M., Almutairi, A.M., Albalawi, K., Dakhilallah, O.K., Zakaly, H.M.H., Ene, A., Abulyazied, D.E., Ahmed, S.M., Youness, R.A., Taha, M.A., 2023. Production of hybrid nanocomposites based on iron Waste reinforced with niobium Carbide/Granite Nanoparticles with Outstanding strength and wear resistance for Use in Industrial applications. Nanomaterials 13, 537. https://doi.org/10.3390/NANO13030537, 2023, Vol. 13, Page 537.

Issa, S.A.M., Rashad, M., Zakaly, H.M.H., Tekin, H.O., Abouhaswa, A.S., 2020. Nb2O5-Li2O-Bi2O3-B2O3 novel glassy system: evaluation of optical, mechanical, and gamma shielding parameters. J. Mater. Sci. Mater. Electron. 31, 22039–22056. https://doi.org/10.1007/s10854-020-04707-7.

Issa, S.A.M., Saddeek, Y.B., Tekin, H.O., Sayyed, M.I., Shaaban, K.S., 2018. Investigations of radiation shielding using Monte Carlo method and elastic properties of PbO-SiO2-B2O3-Na2O glasses. Curr. Appl. Phys. https://doi.org/10.1016/j.cap.2018.02.018.

Kaur, T., Sharma, J., Singh, T., 2019. Experimental evaluation of gamma rays shielding parameters for Zn-Cd-Sn-Pb quaternary alloy. Radiat. Phys. Chem. 156, 193–198. https://doi.org/10.1016/J.RADPHYSCHEM.2018.11.010.

Khalil, A., Bondouk, I.I., Allam, E.A., Nabil, I.M., Al-Abyad, M., Saudi, H., El-Taher, A., Mahmoud, M.E., Amar, A., 2024. A binary composite material of nano polyaniline intercalated with Nano-Fe2O3 for enhancing gamma-radiation-shielding properties: experimental and simulation study. Prog. Nucl. Energy 169, 105067. https://doi.org/10.1016/J.PNUCENE.2024.105067.

Khanna, A., Bhatti, S.S., Singh, K.J., Thind, K.S., 1996. Gamma-ray attenuation coefficients in some heavy metal oxide borate glasses at 662 keV. Nucl. Instrum. Methods Phys. Res., Sect. B 114, 217–220. https://doi.org/10.1016/0168-583X(96)00196-6.

Kilic, G., Ilik, E., Issa, S.A.M., Issa, B., Issever, U.G., Zakaly, H.M.H., Tekin, H.O., 2021. Fabrication, structural, optical, physical and radiation shielding characterization of indium (III) oxide reinforced 85TeO2-(15–x)ZnO-xIn2O3 glass system. Ceram. Int. 47, 27305–27315. https://doi.org/10.1016/j.ceramint.2021.06.152.

Kurudirek, M., 2017. Heavy metal borate glasses: potential use for radiation shielding. J. Alloys Compd. 727, 1227–1236. https://doi.org/10.1016/j.jallcom.2017.08.237.

Liu, J., Xu, X., Zheng, T., Guo, Y., Lv, J., 2022. Effect of Bi2O3 content on the structure and properties of Bi2O3-B2O3-BaO-ZnO glass. J. Non-Cryst. Solids 575, 121211. https://doi.org/10.1016/J.JNONCRYSOL.2021.121211.

Mahmoud, I.S., Issa, S.A.M., Zakaly, H.M.H., Saudi, H.A., Ali, A.S., Saddeek, Y.B., Alharbi, T., Tekin, H.O., 2021. Material characterization of WO3/Bi2O3 substituted calcium-borosilicate glasses: structural, physical, mechanical properties and gamma-ray resistance competencies. J. Alloys Compd. 888 https://doi.org/10.1016/j.jallcom.2021.161419.

Makishima, A., Mackenzie, J.D., 1973. Direct calculation of Young's modulus of glass. J. Non-Cryst. Solids 12, 35–45. https://doi.org/10.1016/0022-3093(73)90053-7.

Manjunatha, H.C., Sathish, K.V., Seenappa, L., Gupta, D., Cecil Raj, S.A., 2019. A study of X-ray, gamma and neutron shielding parameters in Si- alloys. Radiat. Phys. Chem. 165, 108414 https://doi.org/10.1016/J.RADPHYSCHEM.2019.108414.

Mann, K.S., Rani, A., Heer, M.S., 2015a. Shielding behaviors of some polymer and plastic materials for gamma-rays. Radiat. Phys. Chem. 106, 247–254. https://doi.org/10.1016/J.RADPHYSCHEM.2014.08.005.

Mann, K.S., Rani, A., Heer, M.S., 2015b. Shielding behaviors of some polymer and plastic materials for gamma-rays. Radiat. Phys. Chem. 106, 247–254. https://doi.org/10.1016/j.radphyschem.2014.08.005.

Møller, A.P., Mousseau, T.A., 2013. The effects of natural variation in background radioactivity on humans, animals and other organisms. Biol. Rev. 88, 226–254. https://doi.org/10.1111/J.1469-185X.2012.00249.X.

Mostafa, A.M.A., Uosif, M.A.M., Issa, S.A.M., Zhukovsky, M., Alrowaili, Z.A., Zakaly, H. M.H., 2024. Evaluation of photon, proton, and alpha interaction parameters of EDTMPLu and MDPLu medications used for some bone cancer. Radiat. Phys. Chem. 216, 111419 https://doi.org/10.1016/j.radphyschem.2023.111419.

Ogawa, M., Nakajima, Y., Kubota, R., Endo, Y., 2008a. Two cases of acute lead poisoning due to occupational exposure to lead. Clin. Toxicol. 46, 332–335. https://doi.org/10.1080/15563650701816448.

Ogawa, M., Nakajima, Y., Kubota, R., Endo, Y., 2008b. Two cases of acute lead poisoning due to occupational exposure to lead. Clin. Toxicol. 46, 332–335. https://doi.org/10.1080/15563650701816448.

Rammah, Y.S., Issa, S.A.M., Zakaly, H.M.H., Tekin, H.O., Yousef, E., Abouhaswa, A.S., 2021. B2O3-Bi2O3-Li2O3-Cr2O3 glasses: fabrication, structure, mechanical, and gamma radiation shielding qualities. J. Australas. Ceram. Soc. 57, 1057–1069. https://doi.org/10.1007/s41779-021-00599-w.

Rammah, Y.S., Olarinoye, I.O., El-Agawany, F.I., El-Adawy, A., Gamal, A., Yousef, E.S., 2020. Elastic moduli, photon, neutron, and proton shielding parameters of tellurite bismo-vanadate (TeO2–V2O5–Bi2O3) semiconductor glasses. Ceram. Int. 46, 25440–25452. https://doi.org/10.1016/j.ceramint.2020.07.014.

Şakar, E., Özpolat, Ö.F., Alım, B., Sayyed, M.I., Kurudirek, M., 2020. Phy-X/PSD: Development of a user friendly online software for calculation of parameters relevant to radiation shielding and dosimetry. Radiat. Phys. Chem. 166, 108496 https://doi.org/10.1016/j.radphyschem.2019.108496.

Salem, M.M., Kenawy, E.R., Zakaly, H.M.H., Ene, A., Azaam, M.M., Edries, T.B., Zhou, D., Hussein, M.M., Abd El-Hameed, A.S., Nabil, I.M., Darwish, M.A., 2023. Electrospun PVDF/Barium hexaferrite fiber composites for enhanced electromagnetic shielding in the X-band range. Results Phys. 53 https://doi.org/10.1016/J.RINP.2023.106975.

Sayyed, M.I., 2016. Investigation of shielding parameters for smart polymers. Chin. J. Phys. 54, 408–415. https://doi.org/10.1016/J.CJPH.2016.05.002.

Sayyed, M.I., Tekin, H.O., Altunsoy, E.E., Obaid, S.S., Almatari, M., 2018. Radiation shielding study of tellurite tungsten glasses with different antimony oxide as transparent shielding materials using MCNPX code. J. Non-Cryst. Solids 498, 167–172. https://doi.org/10.1016/j.jnoncrysol.2018.06.022.

Shaaban, E.R., Saddeek, Y.B., Abdel Rafea, M., 2009. Crystallization kinetics of the TeO2-BaO glass system. Philos. Mag. A 89, 27–39. https://doi.org/10.1080/14786430802566406.

Singh, H., Singh, Kulwant, Gerward, L., Singh, Kanwarjit, Sahota, H.S., Nathuram, R., 2003. ZnO–PbO–B2O3 glasses as gamma-ray shielding materials. Nucl. Instrum. Methods Phys. Res., Sect. B 207, 257–262. https://doi.org/10.1016/S0168-583X(03)00462-2.

Singh, N., Singh, K.J., Singh, K., Singh, H., 2004. Comparative study of lead borate and bismuth lead borate glass systems as gamma-radiation shielding materials. Nucl. Instrum. Methods Phys. Res., Sect. B 225, 305–309. https://doi.org/10.1016/j.nimb.2004.05.016.

Singh, V.P., Badiger, N.M., Chanthima, N., Kaewkhao, J., 2014. Evaluation of gamma-ray exposure buildup factors and neutron shielding for bismuth borosilicate glasses. Radiat. Phys. Chem. 98, 14–21. https://doi.org/10.1016/j.radphyschem.2013.12.029.

Som, T., Karmakar, B., 2011. Nano silver: antimony glass hybrid nanocomposites and their enhanced fluorescence application. Solid State Sci. 13, 887–895. https://doi.org/10.1016/j.solidstatesciences.2011.02.021.

Tekin, H.O., Ali, F.T., Almisned, G., Susoy, G., Issa, S.A.M., Ene, A., Elshami, W., Zakaly, H.M.H., 2022a. Multiple Assessments on the gamma-ray protection properties of niobium-doped borotellurite glasses: a Wide range investigation using Monte Carlo simulations. Sci. Technol. Nucl. Install. 2022, 1–17. https://doi.org/10.1155/2022/5890896.

Tekin, Huseyin O., Almisned, G., Susoy, G., Ali, F.T., Baykal, D. Sen, Ene, A., Issa, S.A.M., Rammah, Y.S., Zakaly, H.M.H., 2022b. Transmission factor (TF) behavior of Bi2O3–TeO2–Na2O–TiO2–ZnO glass system: a Monte Carlo simulation study. Sustainability 14, 2893. https://doi.org/10.3390/su14052893.

Tekin, Huseyin Ozan, Almisned, G., Susoy, G., Zakaly, H.M.H., Issa, S.A.M., Kilic, G., Rammah, Y.S., Lakshminarayana, G., Ene, A., 2022c. A detailed investigation on highly dense CuZr bulk metallic glasses for shielding purposes. Open Chem. 20, 69–80. https://doi.org/10.1515/chem-2022-0127.

Tekin, Huseyin Ozan, Almisned, G., Zakaly, H.M.H., Zamil, A., Khoucheich, D., Bilal, G., Al-Sammarraie, L., Issa, S.A.M., Al-Buriahi, M.S., Ene, A., 2022d. Gamma, neutron, and heavy charged ion shielding properties of Er3+-doped and Sm3+-doped zinc borate glasses. Open Chem. 20, 130–145. https://doi.org/10.1515/CHEM-2022-0128.

Tekin, H.O., Bilal, G., Zakaly, H.M.H., Kilic, G., Issa, S.A.M., Ahmed, E.M., Rammah, Y.S., Ene, A., 2021. Newly developed vanadium-based glasses and their potential for nuclear radiation shielding aims: a Monte Carlo study on gamma ray attenuation parameters. Materials 14, 3897. https://doi.org/10.3390/ma14143897.

Tekin, H.O., Issa, S.A.M., Ahmed, E.M., Rammah, Y.S., 2022e. Lithium-fluoro borotellurite glasses: Nonlinear optical, mechanical characteristics and gamma radiation protection characteristics. Radiat. Phys. Chem. 190, 109819 https://doi.org/10.1016/J.RADPHYSCHEM.2021.109819.

Zaid, M.H.M., Matori, K.A., Abdul Aziz, S.H., Zakaria, A., Ghazali, M.S.M., 2012. Effect of ZnO on the physical properties and optical band gap of soda lime silicate glass. Int. J. Mol. Sci. 13, 7550–7558. https://doi.org/10.3390/ijms13067550.

Zakaly, H.M., Abouhaswa, A.S., Issa, S.A.M., Mostafa, M.Y.A., Pyshkina, M., El-Mallawany, R., 2020. Optical and nuclear radiation shielding properties of zinc borate glasses doped with lanthanum oxide. J. Non-Cryst. Solids 543, 120151. https://doi.org/10.1016/j.jnoncrysol.2020.120151.

Zakaly, H.M.H., Issa, S.A.M., Tekin, H.O., Badawi, A., Saudi, H.A., Henaish, A.M.A., Rammah, Y.S., 2022. An experimental evaluation of CdO/PbO-B2O3 glasses containing neodymium oxide: structure, electrical conductivity, and gamma-ray resistance. Mater. Res. Bull. 111828 https://doi.org/10.1016/j.materresbull.2022.111828.

Zakaly, H.M.H., Nabil, I.M., Issa, S.A.M., Almousa, N., Khattari, Z.Y., Rammah, Y.S., 2023a. Probing the elasticity and radiation protection potential of neodymium(III) doped zinc and niobium tellurite glasses: an integrated simulated and applied physics perspective. Mater. Today Commun. 37, 107113 https://doi.org/10.1016/j.mtcomm.2023.107113.

Zakaly, H.M.H., Rammah, Y.S., Issa, S.A.M., Almousa, N., El-Refaey, A.M., Shams, M.S., 2023b. Exploring elastic mechanics and radiation shielding efficacy in neodymium (III)-enhanced zinc tellurite glasses: a theoretical and applied physics perspective. J. Theor. Appl. Phys. 17 https://doi.org/10.57647/J.JTAP.2023.1704.44.

Zakaly, H.M.H., Rashad, M., Tekin, H.O., Saudi, H.A., Issa, S.A.M., Henaish, A.M.A., 2021a. Synthesis, optical, structural and physical properties of newly developed dolomite reinforced borate glasses for nuclear radiation shielding utilizations: an experimental and simulation study. Opt. Mater. 114, 110942 https://doi.org/10.1016/j.optmat.2021.110942.

Zakaly, H.M.H., Saudi, H.A., Issa, S.A.M., Rashad, M., Elazaka, A.I., Tekin, H.O., Saddeek, Y.B., 2021b. Alteration of optical, structural, mechanical durability and nuclear radiation attenuation properties of barium borosilicate glasses through BaO reinforcement: experimental and numerical analyses. Ceram. Int. 47, 5587–5596. https://doi.org/10.1016/j.ceramint.2020.10.143.

Zakaly, H.M.H., Tekin, H.O., Issa, A.M.S., Alrowaily, A.W., Ene, A., Rammah, Y.S., 2023c. Dual impacts of Bi2O3/B2O3 substitution on mechanical and attenuation properties of zinc–bismuth–borate Ternary glasses for Diagnosis γ-rays shielding materials application. J. Inorg. Organomet. Polym. Mater. 1–12. https://doi.org/10.1007/s10904-022-02527-2.